Passivation of Current-Controlled Grid-Connected VSCs Using Passivity Indices

Hans, Florian; Schumacher, Walter; Chou, Shih Feng; Wang, Xiongfei

Published in:
IEEE Transactions on Industrial Electronics

DOI (link to publication from Publisher):
10.1109/TIE.2018.2883261

Publication date:
2019

Document Version
Accepted author manuscript, peer reviewed version

Passivation of Current-Controlled Grid-Connected VSCs Using Passivity Indices

Florian Hans, *Student Member, IEEE*, Walter Schumacher, *Member, IEEE*, Shih-Feng Chou, *Member, IEEE*, and Xiongfei Wang, *Senior Member, IEEE*

***Abstract*—Passivity-based analysis and controller design offer a promising approach to guarantee the stability of power systems. If all grid-connected components act strictly passive, critical oscillations cannot arise. Recent research established design guidelines for current-controlled voltage-source converters (VSCs) that allow obtaining a non-negative real part of the converter input admittance for a wide frequency range. In this paper, the findings are extended and generalized from a control engineering point of view. Utilizing passivity indices to quantify the degree of the input admittance's passivity, the current controller design is reviewed and assessed. Further, generic and necessary passivation design criteria are proposed and carried out exemplarily for passive as well as for active damping using voltage feed-forward filters. Finally, the theoretical findings are validated by experiments.**

***Index Terms*—Converter control, passivity, resonances, stabilization, voltage-source converter (VSC).**

I. Introduction

With the rapid increase of sustainable and distributed renewable energy sources, grid-connected voltage source-source converters (VSCs) have become a key component in present power systems. However, the interactions between one VSC, or multiple VSCs, with poorly damped grid resonances are known to cause oscillations or even to destabilize the power system [1], [2]. In fact, the current control as well as the total time delay introduced by the computation plus pulsewidth modulation (PWM) were identified as one of the main reasons for exciting high-frequency harmonic resonances or resonances near to the fundamental grid frequency [2]–[4].

Interpreting the small-signal VSC dynamics as a frequency-dependent converter input admittance that is interconnected to a grid impedance, harmonic stability is most frequently analyzed by applying the Nyquist stability criterion [2], [5]–[8]. This impedance-based method can also be extended to networks that consist of multiple power converters [8]. Nevertheless, since each VSC contributes to the power system stability, every network has to be analyzed individually, and thus, it is not possible to deduce general stability statements.

Manuscript received May 11, 2018; revised September 10, 2018; accepted November 02, 2018.

F. Hans and W. Schumacher are with the Institute of Control Engineering, Technische Universität Braunschweig, 38106 Braunschweig, Germany (e-mail: hans@ifr.ing.tu-bs.de; w.schumacher@tu-bs.de).

S.-F. Chou and X. Wang are with the Department of Energy Technology, Aalborg University, Aalborg 9220, Denmark (e-mail: shc@et.aau.dk; xwa@et.aau.dk).

On the other hand, passivity-based control [9], [10] represents a powerful approach allowing to apply passivity theorems which give sufficient conditions for power system stability, despite of the configuration and number of grid-connected VSCs. Assuming that the power network only consists of passive components, stability is guaranteed by design, if all grid-connected converters are passive, i.e., the real part of each converter input admittance is non-negative.

Among others, especially Harnefors et al. investigated the frequency-domain passivity-based controller design and stability assessment of grid-connected VSCs, see e.g., [3], [4], [11], [12]. If any computation and PWM time delay is neglected, it is easy to achieve a non-negative real part of the input admittance for all frequencies and various controllers [11]. However, considering non-idealized, practical conditions, a passive input admittance for all frequencies is hard to obtain and additional damping has to be introduced [3], [4], [12], [13]. Regarding present standards, e.g., the railway standard EN 50388-2 [14], typical requirements enforce dissipative active-front-ends up to the Nyquist frequency, while latest works motivate a non-negative real part of the input admittance even above the Nyquist frequency, see e.g., [12].

Nevertheless, even though the authors of [3] proposed an active damping control scheme, that is based on a stationary-frame proportional-resonant (PR) current controller with point of common coupling (PCC) voltage feed-forward, the feed-forward filter design still lacks a thorough scientific investigation. In particular, the question has to be answered, which filter types are able to render the real part of the input admittance non-negative, and moreover, generic filter design guidelines would be desirable. In addition, common literature, e.g., [3], [4], [11]–[13], concentrates on methods that achieve a passive VSC input admittance. From a practical point of view, this design may be sufficient to prevent critical oscillations, but can also be extended to obtain strictly passive components, allowing to guarantee asymptotic stability of the power system.

Hence, this paper aims to extend the findings of frequency-domain passivity-based controller design and stability assessment of grid-connected VSCs. Using passivity indices, which allow to quantify the degree of a system's passivity, the topic is rounded off from a more system-theoretic point of view. The main contributions are twofold. After giving the background on passivity theory and introducing the VSC system under study, in Section IV-A, the current controller design is reviewed. Besides introducing an analytical method for passive damping dimensioning, it is shown that damped

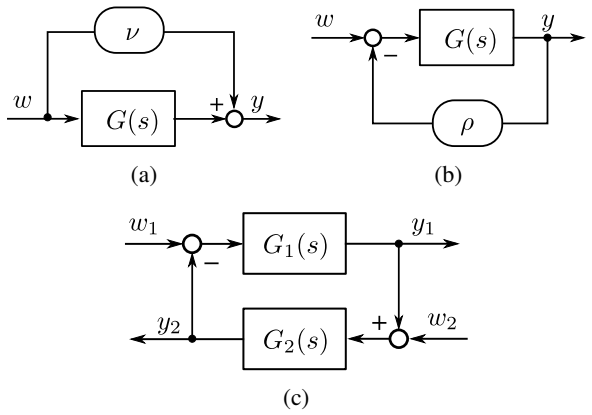

Fig. 1: Passivation of $G(s)$ (a) with $\mathrm{IFP}\,(G) = -\nu$ by input feed-forward and (b) with $\mathrm{OFP}\,(G) = -\rho$ by output feedback. (c) Feedback interconnection of passive subsystems.

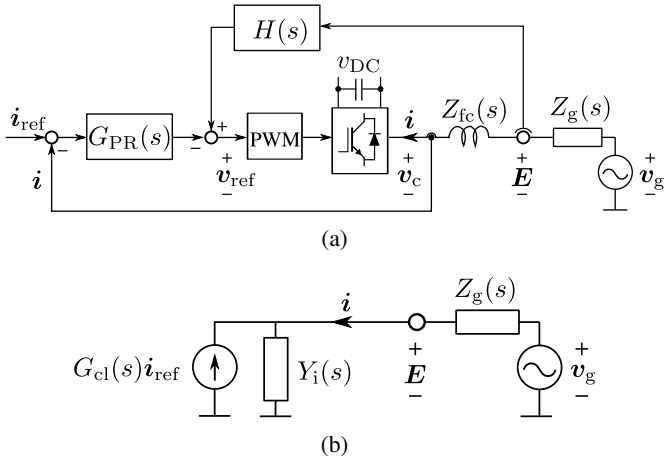

Fig. 2: (a) Single-phase equivalent block diagram and (b) impedance-based equivalent circuit diagram of a grid-connected VSC with PCC voltage feed-forward filter.

PR controllers are beneficial to obtain a passive system and are necessary to render the input admittance strictly passive. Secondly, in Section IV-B, generic and necessary passivation design criteria for VSCs with PCC voltage feed-forward filters are derived and carried out exemplarily.

II. Frequency-Domain Passivity Theory

A. Passivity of Linear Systems

A linear single-input single-output (SISO) system with transfer function $G(s)$ is said to be passive, if 1) $G(s)$ is stable, i.e., $\mathrm{Re}\,\{p_i\} \leq 0$, $i = 1, \ldots, n$, were p_i are the poles of $G(s)$ and 2) the real part of the frequency response is always nonnegative, i.e., $\mathrm{Re}\,\{G(j\omega)\} \geq 0$, $\forall \omega \in \mathbb{R}$. Moreover, $G(s)$ is said to be strictly passive, if 1) $G(s)$ is Hurwitz, i.e., $\mathrm{Re}\,\{p_i\} < 0$, $i = 1, \ldots, n$, 2) $\mathrm{Re}\,\{G(j\omega)\} > 0$, $\forall \omega \in \mathbb{R}$, 3) $G(\infty) \geq 0$, and 4) $\lim\limits_{\omega \to \infty} \omega^2 \mathrm{Re}\,\{G(j\omega)\} > 0$ [9], [10].

Equivalently, the phase response of each stable SISO passive system lies always within $[-90°, 90°]$ and the phase response of a SISO strictly passive system is always within $(-90°, 90°)$.

B. Passivity Indices and Passivation

If passive or nonpassive subsystems are combined, passivity indices can be utilized to quantify the degree of passivity of the resulting system, and thus, help to render a system passive.

The input feed-forward passivity (IFP) index for a stable linear SISO system $G(s)$ is defined by the minimum real part of the frequency response, i.e., $\mathrm{IFP}\,(G) = \nu = \min_{\omega \in \mathbb{R}} \mathrm{Re}\,\{G(j\omega)\}$. Similarly, the output feedback passivity (OFP) index for a minimum phase system is defined by $\mathrm{OFP}\,(G) = \rho = \min_{\omega \in \mathbb{R}} \mathrm{Re}\,\{G^{-1}(j\omega)\}$ [9]. As illustrated in Fig. 1a, if ν is negative, then the system shows a shortage of passivity and can be rendered passive by employing a minimum positive feed-forward of ν. Graphically examined, the passivation by input feed-forward shifts the Nyquist plot of $G(j\omega)$ by ν in the right direction, such that $\mathrm{Re}\,\{G(j\omega)\} \geq 0$, $\forall \omega \in \mathbb{R}$. Equally, as shown in Fig. 1b, if ρ is negative, the system lacks passivity and can be rendered passive by employing a minimum negative feedback of ρ, but does not have a direct graphically interpretation.

Moreover, it is possible to specify frequency-dependent passivity indices, i.e., $\nu(\omega) = \mathrm{Re}\,\{G(j\omega)\}$ and $\rho(\omega) = \mathrm{Re}\,\{G^{-1}(j\omega)\}$, which allow for a frequency-domain filter design in Section IV.

C. Passivity Theorems

Since passivity implies stability, each passive system is stable, that is, all poles satisfy $\mathrm{Re}\,\{p_i\} \leq 0$. Further, each strictly passive system is asymptotically stable, i.e, $\mathrm{Re}\,\{p_i\} < 0$.

Considering interconnected systems, two linear passive subsystems that are either connected in parallel or in a feedback-loop both result in a passive system again. Regarding Fig. 1c, the closed-loop system always results in an asymptotically stable system, if the subsystem in the forward path is strictly passive and the subsystem in the feedback path is passive [9], [10]. This can directly be seen from the open-loop Bode plot, where the total phase response never reaches $-180°$, and thus, always satisfies the Nyquist stability criterion.

Remark 1: It should be emphasized that contrary to passivity theory, common literature, e.g., [3], [4], [11], [12], requires a passive VSC input admittance to assess (asymptotic) stability. Even though only strict passivity guarantees asymptotic stability, passive components are often sufficient to prevent the power system from unwanted oscillations.

III. System Model

The contributions of this paper can be applied to single-phase as well as three-phase systems. If three-phase systems are considered, the variables should be interpreted as complex space vectors in stationary (α, β)-coordinates, e.g., $\boldsymbol{v} = v_\alpha + j v_\beta$. For convenience, linear, continuous-time SISO systems are assumed throughout the paper. Moreover, although digitally implemented controllers are supposed, the analysis is performed in the continuous s-domain.

A. Grid-Connected VSCs

Fig. 2a shows the basic current-control structure of a grid-connected VSC. Here, it is assumed that the grid impedance

$Z_{\mathrm{g}}(s)$ represents a resistive-inductive-capacitive (RLC) network that interconnects the VSC to a stiff grid with voltage $\boldsymbol{v}_{\mathrm{g}}$ and fundamental frequency f_{r}, e.g., $50\,\mathrm{Hz}$ or $60\,\mathrm{Hz}$. The converter is equipped with a symmetric resistive-inductive (RL) output filter $Z_{\mathrm{fc}}(s) = R_{\mathrm{fc}} + sL_{\mathrm{fc}}$, where R_{fc} and L_{fc} are the output filter resistance and inductance, respectively. Hence, the dynamics of the controlled grid current $\boldsymbol{i}$ in the Laplace domain are given by

$$\begin{aligned}\boldsymbol{i}(s) &= Y_{\mathrm{fc}}(s)\left(\boldsymbol{E}(s) - \boldsymbol{v}_{\mathrm{c}}(s)\right)\\ &= \frac{1/R_{\mathrm{fc}}}{L_{\mathrm{fc}}/R_{\mathrm{fc}}s + 1}\left(\boldsymbol{E}(s) - \boldsymbol{v}_{\mathrm{c}}(s)\right)\end{aligned} \tag{1}$$

where $\boldsymbol{E}$ represents the voltage at the PCC and $\boldsymbol{v}_{\mathrm{c}}$ is the VSC output voltage.

Supposing that the converter always operates within its permissible voltage range and overmodulation does not occur, the converter plus PWM unit is typically approximated by the average model $\boldsymbol{v}_{\mathrm{c}}(s) = e^{-sT_{\mathrm{d}}}\boldsymbol{v}_{\mathrm{ref}}(s)$, where $\boldsymbol{v}_{\mathrm{ref}}$ is the desired converter voltage and T_{d} is the associated computation plus PWM time delay [3], [4], [6], [8], [13], [15]–[17]. Due to the synchronous sampling with the PWM cycle, switching harmonics are effectively damped and antialiasing analog-to-digital converter prefiltering can be avoided [3], [4]. For typical two-level VSCs that implement synchronous current sampling with sampling time T_{s} and computation time T_{c}, the (maximum) total time delay is $T_{\mathrm{d}} = T_{\mathrm{c}} + T_{\mathrm{s}}/2$. Commonly, the update instant of $\boldsymbol{v}_{\mathrm{ref}}$ is delayed by the sampling period, yielding a delay of $T_{\mathrm{d}} = 1.5\,T_{\mathrm{s}}$. The latter assumption can be considered as a worst-case approximation, which, in many cases, gives too conservative results [4], [12], [15].

Alternatively to a pure time delay, a zero-order-hold (ZOH) element can be used as a more accurate PWM model [12], [15]. In doing so, the converter model, consisting of the PWM and an associated computation time is modeled by

$$\boldsymbol{v}_{\mathrm{c}}(s) = G_{\mathrm{d}}(s)\boldsymbol{v}_{\mathrm{ref}}(s) = e^{-sT_{\mathrm{s}}}\frac{1 - e^{-sT_{\mathrm{s}}}}{sT_{\mathrm{s}}}\boldsymbol{v}_{\mathrm{ref}}(s), \tag{2}$$

where the first term takes the processing delay $T_{\mathrm{c}} = T_{\mathrm{s}}$ into account. While the phase shift of $e^{-s\,1.5T_{\mathrm{s}}}$ is identical to the phase shift of (2) for frequencies below the sampling frequency $\omega_{\mathrm{s}} = 2\pi/T_{\mathrm{s}}$, the magnitude of (2) decreases from 1 at $\omega = 0\,\mathrm{rad/s}$ to 0 at $\omega = \omega_{\mathrm{s}}$. This property relaxes the worst-case PWM approximation, especially close and above the Nyquist frequency $\omega_{\mathrm{N}} = \omega_{\mathrm{s}}/2$ [12].

Then, using an (α, β)-frame PR current controller with a transfer function $G_{\mathrm{PR}}(s)$ to regulate the grid current $\boldsymbol{i}$ and implementing an additional active damping feed-forward filter $H(s)$, the VSC output voltage is calculated by

$$\boldsymbol{v}_{\mathrm{c}}(s) = G_{\mathrm{d}}(s)\left[-G_{\mathrm{PR}}(s)(\boldsymbol{i}_{\mathrm{ref}}(s) - \boldsymbol{i}(s)) + H(s)\boldsymbol{E}(s)\right] \tag{3}$$

where $\boldsymbol{i}_{\mathrm{ref}}$ is the reference current. To be consistent with [3], [4], [11], the current $\boldsymbol{i}$ is defined to flow in the direction of the converter, which results in the negative sign of the first term in (3).

B. Impedance-Based Equivalent Circuit

Interpreting the VSC in terms of electrical circuit components, the system of Fig. 2a can be understood as a controlled current source that is connected to the grid [2]–[5], [11], [13], as shown in Fig. 2b. Here, $G_{\mathrm{cl}}(s)$ represents the closed-loop transfer function between the reference current $\boldsymbol{i}_{\mathrm{ref}}$ and the injected grid current $\boldsymbol{i}$, while Y_{i}(s) is the (inner) input admittance, which describes the disturbance behavior from $\boldsymbol{E}$ to $\boldsymbol{i}$. Given (1) and (3), the dynamic behavior of the current source in the Laplace domain can be described by the single-frequency model

$$\boldsymbol{i}(s) = G_{\mathrm{cl}}(s)\boldsymbol{i}_{\mathrm{ref}}(s) + Y_{\mathrm{i}}(s)\boldsymbol{E}(s) \tag{4}$$

with

$$G_{\mathrm{cl}}(s) = \frac{G_{\mathrm{PR}}(s)G_{\mathrm{d}}(s)Y_{\mathrm{fc}}(s)}{1 + G_{\mathrm{PR}}(s)G_{\mathrm{d}}(s)Y_{\mathrm{fc}}(s)} \tag{5}$$

$$Y_{\mathrm{i}}(s) = \left[1 - H(s)G_{\mathrm{d}}(s)\right]\frac{Y_{\mathrm{fc}}(s)}{1 + G_{\mathrm{PR}}(s)G_{\mathrm{d}}(s)Y_{\mathrm{fc}}(s)}, \tag{6}$$

where aliasing effects are disregarded [12]. Referring to Fig. 2b, the PCC voltage can also be expressed in terms of the grid voltage $\boldsymbol{v}_{\mathrm{g}}$ and the grid current $\boldsymbol{i}$, i.e., $\boldsymbol{E} = \boldsymbol{v}_{\mathrm{g}} - Z_{\mathrm{g}}(s)\,\boldsymbol{i}$. Hence, after substituting, the closed-loop stability of (4) in combination with the grid can be checked by analyzing

$$\boldsymbol{i}(s) = \frac{G_{\mathrm{cl}}(s)}{1 + Y_{\mathrm{i}}(s)Z_{\mathrm{g}}(s)}\boldsymbol{i}_{\mathrm{ref}}(s) + \frac{Y_{\mathrm{i}}(s)}{1 + Y_{\mathrm{i}}(s)Z_{\mathrm{g}}(s)}\boldsymbol{v}_{\mathrm{g}}(s). \tag{7}$$

Since the reference transfer function $G_{\mathrm{cl}}(s)$ is designed to be stable, the overall system stability is assured if the open-loop plot of the grid impedance multiplied with the input admittance, also referred to as the minor-loop gain, satisfies the Nyquist stability criterion [5]–[8]. However, assuming that the connected RLC network only consists of (strictly) passive elements, $Z_{\mathrm{g}}(s)$ is also (strictly) passive. Hence, according to Section II-C and Fig. 1c, stability can be obtained if the VSC also represents a passive system, i.e., the input admittance $Y_{\mathrm{i}}(s)$ shows a non-negative real part [3], [4], [11], [13], while asymptotic stability is guaranteed, if $Y_{\mathrm{i}}(s)$ is strictly passive.

Remark 2: Although the definition of passivity requires that the criteria of Section II-A are fulfilled for all $\omega \in \mathbb{R}$, standards like the EN50388-2 [14] enforce dissipative active front-ends up to the Nyquist frequency ω_{N}. Hence, throughout this paper, the passivity analysis is performed with respect to the domain $\mathbb{D} = [0, \omega_{\mathrm{N}}]$ [3], [4], [11], [13], which implies that condition 3) and 4) of Section II-A, which define whether a system is strictly passive or not, can be omitted.

Remark 3: Because of the discrete implementation of the converter control system, the resulting feedback-loop consists of a discrete and a continuous part, and thus, represents a hybrid sampled-data system [18]. However, since this paper aims to present the theoretical passivity background to previous research and to propose a new controller and filter design idea, sampling effects are disregarded and shall be addressed in future contributions. In this context, [12] provides an initial analysis of sampling effects that suggests to implement an input admittance, which also has a non-negative real part above the Nyquist frequency. In doing so, the critical excitation of above-Nyquist-frequency grid resonances can be prevented and a power system destabilization is unlikely to occur. Even though the effects of sampling and aliasing require further

This article has been accepted for publication in a future issue of this journal, but has not been fully edited. Content may change prior to final publication. Citation information: DOI 10.1109/TIE.2018.2883261, IEEE Transactions on Industrial Electronics

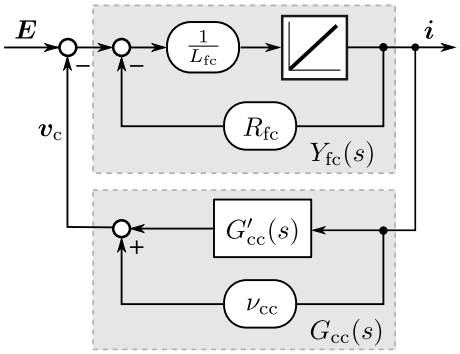

Fig. 3: Block diagram of the input admittance $Y_{\rm i}(s)$ without active filters.

scientific investigation, the findings of [12] can, if required, be taken into account by extending the domain $\mathbb{D}$.

IV. Controller Design

Even though a purely current-controlled converter is not passive in general, the input admittance $Y_{\rm i}(s)$ of the VSC system in Fig. 2a can be rendered passive by introducing sufficient damping by the resistance $R_{\rm fc}$ or implementing an additional feed-forward filter $H(s)$. In this section, necessary passivation design guidelines are proposed using passivity indices. Moreover, the findings are extended to converters that are equipped with inductive-capacitive-inductive (LCL) output filters.

A. Current Controller

Starting with a purely current-controlled converter without any additional feed-forward filter, i.e., $H(s) = 0$, the input admittance (6) can be interpreted as a feedback interconnection of the RL filter admittance $Y_{\rm fc}(s)$ in the forward path and the series connection of the PR controller plus converter model, $G_{\rm cc}(s) = G_{\rm PR}(s)G_{\rm d}(s)$, in the feedback path. Given (1), it can be observed that $\mathrm{OFP}\,(Y_{\rm fc}) = \rho_{\rm fc} = R_{\rm fc} = \text{const.}$ Further, supposing that $G_{\rm cc}(s)$ shows a frequency-dependent IFP index of $\mathrm{IFP}\,(G_{\rm cc}) = \nu_{\rm cc}(\omega)$, $G_{\rm cc}(s)$ can be decomposed into a passive system with $\mathrm{IFP}\,(G'_{\rm cc}) = \nu'_{\rm cc}(\omega) = 0$ plus an input feed-forward element with IFP index $\nu_{\rm cc}(\omega)$. Then, with respect to Section II-B and similar to the idea of [13], where the input admittance has been decomposed as a passive filter and an active admittance, $Y_{\rm i}(s)$ can be represented as a feedback interconnection as shown in Fig. 3. Since both, the integrator as well as $G'_{\rm cc}(s)$ are passive elements with $\mathrm{Re}\,\{G(j\omega)\} = 0, \forall\omega \in \mathbb{D}$, the system in Fig. 3 will be (strictly) output passive, if

$$\mathrm{OFP}\,(Y_{\rm i}) = \mathrm{OFP}\,(Y_{\rm fc}) + \mathrm{IFP}\,(G_{\rm cc}) \Leftrightarrow R_{\rm fc} + \nu_{\rm cc}(\omega) \geq 0, \forall\omega \in \mathbb{D}. \tag{8}$$

Remark 4: While (8) is derived by means of passivity indices, [12] also presents the condition as a necessary requirement for stability, using the Nyquist stability criterion. In this context, the system decomposition of Section IV-A gives the system-theoretic interpretation of the findings from [12].

TABLE I: Test-system parameters

Parameter	Symbol	Value	Units
Grid voltage	$\lvert\boldsymbol{v}_{\rm g}\rvert$	400	V
Fundamental frequency	$f_{\rm r}$	50	Hz
Sampling frequency	$f_{\rm s}$	10	kHz
Total time delay	$T_{\rm d}$	0.15	ms
Filter inductance	$L_{\rm fc}$	3	mH
Filter resistance	$R_{\rm fc}$	0.2	Ω

1) Ideal PR Controller: Focusing on reference current tracking, the transfer function of an ideal PR current controller with phase compensation is given by

$$G_{\rm PR}(s) = K_{\rm P} + K_{\rm I}\frac{s\cos(\phi) - \omega_{\rm r}\sin(\phi)}{s^2 + \omega_{\rm r}^2} \tag{9}$$

where $\omega_{\rm r} = 2\pi f_{\rm r}$ is the resonant frequency, $K_{\rm P}$ is the proportional gain in Ω, $K_{\rm I}$ is the integral gain in Ω/s, and ϕ represents the compensation angle allowing to introduce an additional phase lead at $\omega_{\rm r}$. The proportional gain can be selected by common design guidelines, e.g., $K_{\rm P} = \alpha_{\rm c}L_{\rm fc}$, where $\alpha_{\rm c}$ is the desired closed-loop current-control bandwidth, for which $\alpha_{\rm c} \leq \omega_{\rm s}/10$ is recommended [3], [4], [11], [16], [19]. Neglecting the influence of the compensation angle, i.e., $\phi \approx 0°$, the phase margin $\Phi_{\rm m}$ of the open-loop transfer function $G_{\rm o}(s) = G_{\rm PR}(s)G_{\rm d}(s)Y_{\rm fc}(s)$ can be approximated by

$$\Phi_{\rm m} \approx \pi - \tan^{-1}\left(\frac{K_{\rm I}}{\alpha_{\rm c}K_{\rm P}}\right) - \alpha_{\rm c}T_{\rm d} - \frac{\pi}{2}, \tag{10}$$

considering a high crossover frequency $\alpha_{\rm c} \gg \omega_{\rm r}$, and thus, $\tan^{-1}(\alpha_{\rm c}L_{\rm fc}/R_{\rm fc}) \approx \pi/2$. With the approximation $\tan^{-1}(K_{\rm I}/\alpha_{\rm c}K_{\rm P}) \approx K_{\rm I}/\alpha_{\rm c}K_{\rm P}$, it is proposed to select the integral gain with respect to a desired phase margin as

$$K_{\rm I} \approx (\pi/2 - \alpha_{\rm c}T_{\rm d} - \Phi_{\rm m})\alpha_{\rm c}K_{\rm P}. \tag{11}$$

Due to its resonant character, (9) provides an infinite gain at $\omega_{\rm r}$, while the phase response at frequencies infinitely close to $\omega_{\rm r}$ shows an relative phase change of 180° [20]. Using the compensation angle ϕ as an additional degree of freedom, the minimum phase value at $\omega_{\rm r}$ can be increased by ϕ, where $\phi = 0°$ yields the ideal PR controller with a phase jump from $-90°$ to $90°$.

Regarding the series connection of $G_{\rm PR}(s)$ and $G_{\rm d}(s)$, the converter model introduces a phase lag of $\arg\{G_{\rm d}(j\omega)\} = -1.5\,\omega T_{\rm s}$. Hence, the passivity of $G_{\rm cc}(s)$ close to the resonant frequency can be obtained by choosing [3]

$$\phi = \omega_{\rm r}T_{\rm d}, \qquad T_{\rm d} = 1.5\,T_{\rm s}. \tag{12}$$

However, even though the phase lag of $G_{\rm d}(s)$ at $\omega_{\rm r}$ is exactly compensated, $\mathrm{Re}\,\{G_{\rm cc}(j\omega)\} = \nu_{\rm cc}(\omega)$ will become negative for higher frequencies. Thus, condition (8) can only be fulfilled, if the resistance of the RL output filter satisfies

$$\begin{aligned} R_{\rm fc} &\geq \left|\inf_{\omega\in\mathbb{D}} \nu_{\rm cc}(\omega)\right| \\ &\geq \left|\inf_{\omega\in\mathbb{D}} (\mathrm{Re}\,\{G_{\rm PR}\}\mathrm{Re}\,\{G_{\rm d}\} - \mathrm{Im}\,\{G_{\rm PR}\}\mathrm{Im}\,\{G_{\rm d}\})\right|. \end{aligned} \tag{13}$$

This article has been accepted for publication in a future issue of this journal, but has not been fully edited. Content may change prior to final publication. Citation information: DOI 10.1109/TIE.2018.2883261, IEEE Transactions on Industrial Electronics

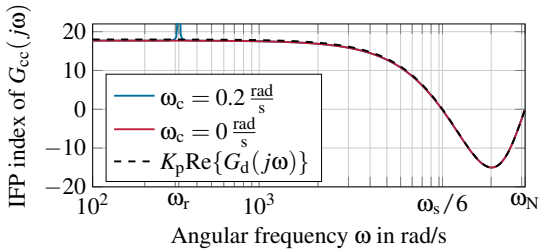

Fig. 4: IFP index of $G_{cc}(j\omega)$ for (red) ideal and (blue) damped PR controller and (black) its high-frequency approximation.

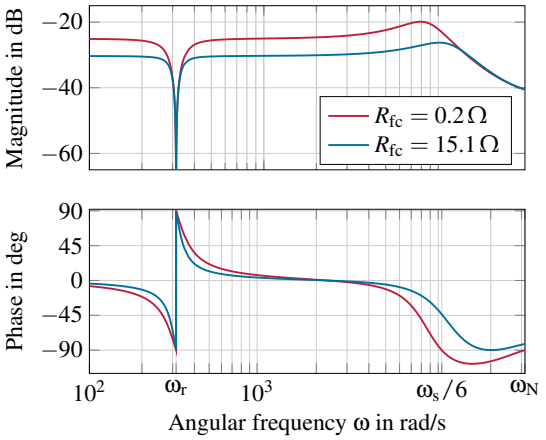

Fig. 5: Bode plots of the VSC input admittance $Y_i(j\omega)$ for different RL filter resistances without active PCC voltage feed-forward filtering.

Example 1: The parameters of a grid-connected VSC are given by Table I. Adopting the suggested design guidelines and choosing a closed-loop current-control bandwidth of $\alpha_c = 6000\,\mathrm{rad/s}$ and a phase margin of $\Phi_m \approx 38°$, the gains are calculated as $K_P = \alpha_c L_{fc} = 18\,\Omega$, $K_I = 0.0185\,\alpha_c^2 L_{fc} = 2000\,\Omega/\mathrm{s}$. Further, using (12) to compensate for the total time delay, i.e., $\phi = 2.7°$, the red evolution in Fig. 4 shows the IFP index of $G_{cc}(j\omega)$. As can be observed, there exists a negative region for frequencies in $[\omega_s/6, \omega_N]$, which also results in an input admittance phase response with $\arg\{Y_i(j\omega)\} \leq -90°$, see the red Bode plot in Fig. 5. Then, referring to Fig. 4 and condition (13), and increasing the filter resistance to e.g., $R_{fc} = 15.1\,\Omega$, the input admittance $Y_i(s)$ is passivated. This is verified by Fig. 5, which shows that the phase response always lies withing $[-90°, 90°]\,, \forall\omega \in \mathbb{D}$.

As demonstrated in Fig. 4 from Example 1, the IFP index of $G_{cc}(j\omega)$ for high frequencies above the fundamental frequency $\omega \geq \omega_s/6$ can be approximated by

$$\nu_{cc}(\omega) \approx K_P \mathrm{Re}\{G_d(j\omega)\} = K_P \frac{2\sin(\omega T_s/2)}{\omega T_s} \cos(\omega T_d). \tag{14}$$

In this context, the resonant part of the PR controller (9) has negligible influence and $G_{cc}(s)$ can be regarded as a series connection of a pure proportional (P) controller and the converter model $G_d(s)$. Observing that, regardless of the switching frequency ω_s, (14) always has a local minimum at $\omega_{min} \approx 2.014/T_s$, the passivation criterion (13) yields the design guideline

$$R_{fc} \approx K_P \mathrm{Re}\{G_d(j\omega_{min})\} \approx 0.84\,K_P. \tag{15}$$

With respect to (13), this simplifies the design process, but may require some empirical fine-tuning. For instance, using the parameters of Example 1, (15) gives a resistance of $R_{fc} = 0.84 \cdot 18\,\Omega = 15.12\,\Omega$, where Fig. 5 illustrates that a lower resistance renders the input admittance passive as well. The deviation increases for lower switching frequencies, since the resonant part of the PR controller in (13) increasingly influences the complex part of the converter model $G_d(s)$.

At this time it becomes also clear that the specified current-control bandwidth is directly related to passivity by choosing the proportional gain K_P. In general, if the bandwidth is increased, more damping has to be introduced, and thus, the passivity of $Y_i(s)$ is harder to obtain. Therefore, a trade-off between fast reference current tracking and disturbance rejection has to be found during the design process.

Remark 5: The identified frequency close to $\omega_s/6$, where the real part of the input admittance becomes negative, was also observed as critical frequency in previous works, e.g., [3], [13]. Given the IFP index of $G_{cc}(j\omega)$ and its approximation (14), this finding can be verified, since $K_P \mathrm{Re}\{G_d(j\omega_s/6)\} = 0$ and $\nu_{cc}(\omega) \approx K_P \mathrm{Re}\{G_d(j\omega)\} < 0$ for $\omega_s/6 < \omega < \omega_N$.

Remark 6: Although the input admittance can be rendered strictly output passive, i.e. $\mathrm{OFP}(Y_i) > 0, \forall\omega \in \mathbb{D}$, this does not imply strict passivity as defined in Section II-A. In general, strict passivity for linear systems requires strict IFP [9]. Observing that $\mathrm{Re}\{Y_i(j\omega_r)\} = 0$ or $\arg\{Y_i(j\omega)\} \in [-90°, 90°]$ for frequencies close to ω_r, despite of the chosen resistance and PR controller gains, the ideal PR controller of (9) is not able to transform the input admittance into a strictly passive system. If strict passivity, and thus, asymptotic stability is required, additional damping at ω_r has to be introduced. This motivates to use a damped PR controller instead.

2) Damped PR Controller: Again focusing on reference current tracking and utilizing ω_c as the resonant cut-off frequency, a damped PR current controller of the form

$$G'_{PR}(s) = K_P + K_I \frac{s\cos(\phi) - \omega_r \sin(\phi)}{s^2 + \omega_c s + \omega_r^2} \tag{16}$$

is proposed. Here, the same controller gain design can be performed as for the standard ideal PR controller, assuming a small resonant cut-off frequency [16]. The converter phase lag at ω_r can again be compensated by (12). Given (16), ω_c represents an additional degree of freedom, which reduces the gain at the resonance frequency to $|G'_{PR}(j\omega_r)| = K_P + K_I/\omega_c$, but also compresses the phase response close to ω_r, yielding $\arg\{G'_{PR}(j\omega)\} \in (-90°, 90°)\,, \forall\omega \in \mathbb{D}$.

Therefore, if $\omega_c > 0$ and the RL filter resistance R_{fc} is chosen according to (13), where the $\geq$ sign is replaced with a $>$ sign, the input admittance $Y_i(s)$ becomes strictly passive.

Example 2: Again supposing the converter system parameters of Table I and the PR controller parameters to be $K_P = 18\,\Omega$, $K_I = 2000\,\Omega/\mathrm{s}$, $\phi = 2.7°$. Then, the blue evolution in Fig. 4 shows the IFP index of $G_{cc}(j\omega)$ using a cut-off frequency of $\omega_c = 0.2\,\mathrm{rad/s}$. A positive peak close

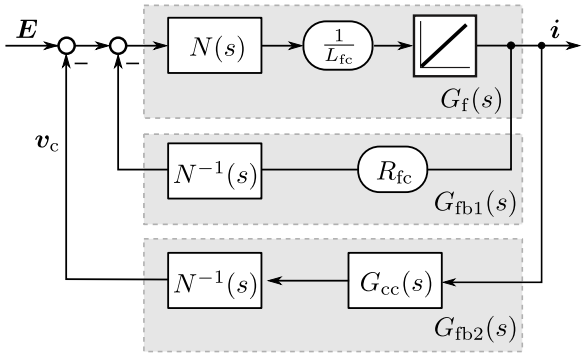

Fig. 6: Block diagram of the input admittance $Y_i(s)$, where the effects of the feed-forward filter are considered by $N(s) = 1 - H(s)G_d(s)$.

to ω_r can be observed, while $\nu_{cc}(\omega)$ matches the red evolution of Example 1 for higher frequencies. Hence, again adopting a resistance of $R_{fc} = 15.1\,\Omega$, the input admittance can be passivated, i.e., $\arg\{Y_i(j\omega)\} \in (-90°, 90°), \forall\omega \in \mathbb{D}$.

Remark 7: In [21], Zmood et al. claimed that a damped PR controller does not have any benefit compared to the ideal implementation. This might be true, if only reference current tracking is considered, but does not apply to disturbance rejection. As demonstrated, the additional damping at ω_r is necessary to render the input admittance strictly passive, and thus, is advantageous to guarantee asymptotic stability of the closed-loop system (7). As it will be shown in the following section, a damped PR controller is also preferable to passivate $Y_i(s)$, if a PCC voltage feed-forward filter is implemented.

B. Feed-Forward Filter Design

In order to avoid a high passive filter resistance, and thus, high losses, an additional feed-forward filter $H(s)$ can be implemented. Observing that (6) consists of a series connection of the system shown in Fig. 3 and a system $N(s) = 1 - H(s)G_d(s)$, after rearranging, $Y_i(s)$ can be represented as a feedback interconnection as shown in Fig. 6. Then, similar to Section IV-A, $Y_i(s)$ will be passive, if

$$\mathrm{OFP}\,(Y_i) = \mathrm{OFP}\,(G_f) + \mathrm{IFP}\,(G_{fb1}) + \mathrm{IFP}\,(G_{fb2}) \geq 0, \forall\omega \in \mathbb{D} \tag{17}$$

where $G_f(s) = \frac{N(s)}{L_{fc}s}$ is the forward system and $G_{fb1}(s) = R_{fc}N^{-1}(s)$, $G_{fb2}(s) = N^{-1}G_{cc}(s)$ are the feedback systems. Regarding the IFP and OFP definitions of Section II-B, (17) can be rewritten as

$$\begin{aligned}\mathrm{OFP}\,(Y_i) &= \mathrm{Re}\left\{jL_{fc}\omega N^{-1}(j\omega)\right\} + \mathrm{Re}\left\{R_{fc}N^{-1}(j\omega)\right\} \\ &\quad + \mathrm{Re}\left\{N^{-1}(j\omega)G_{cc}(j\omega)\right\} \\ &= -L_{fc}\omega\mathrm{Im}\left\{N^{-1}(j\omega)\right\} + R_{fc}\mathrm{Re}\left\{N^{-1}(j\omega)\right\} \\ &\quad + \mathrm{Re}\left\{N^{-1}(j\omega)\right\}\mathrm{Re}\left\{G_{cc}(j\omega)\right\} \\ &\quad - \mathrm{Im}\left\{N^{-1}(j\omega)\right\}\mathrm{Im}\left\{G_{cc}(j\omega)\right\} \geq 0, \forall\omega \in \mathbb{D}.\end{aligned} \tag{18}$$

Here, it should be noticed that (18) represents a set of generic inequalities, which do not depend on a certain PR controller, PWM model nor feed-forward filter. Moreover, (18) does not impose any restrictions on the converter's power rating or sampling frequency. Thus, (18) can be understood as a set of general criteria that have to be fulfilled to passivate the VSC input admittance $Y_i(s)$ in the specified frequency region.

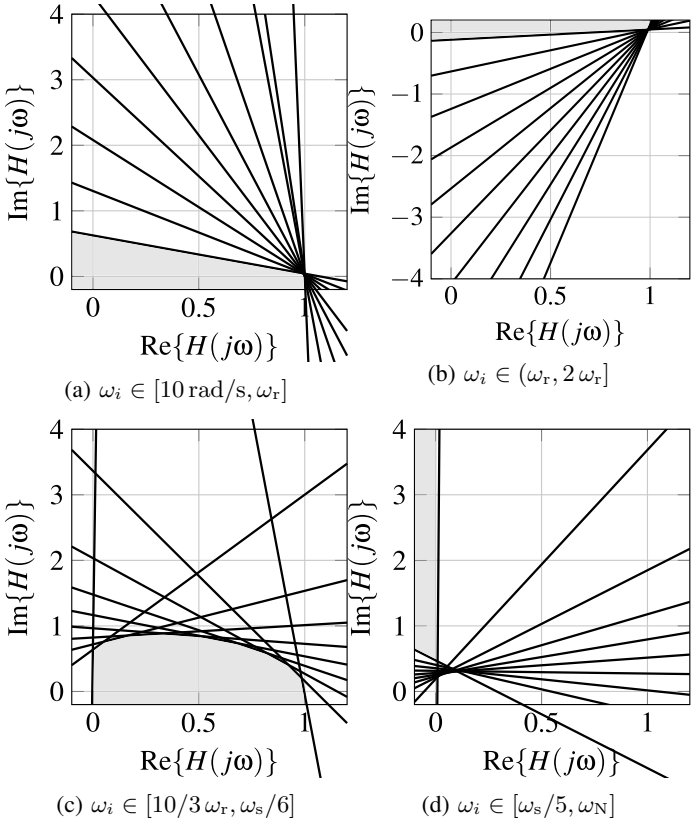

Fig. 7: Exemplary filter criteria for varying frequencies ω_i, where $\mathrm{Im}\{H(j\omega_i)\}$ has to lie below the respective line in (a) and (c) and above in (b) and (d).

1) Criteria in the Complex s-Plane: In order to interpret the criteria that are imposed by (18), it is reasonable to illustrate the inequalities in the complex s-plane. Given the converter model (2), expanding and rearranging (18) yields

$$\mathrm{Im}\{H(j\omega)\} \leq \frac{m_1(\omega)}{m_2(\omega)}\mathrm{Re}\{H(j\omega)\} + \frac{b(\omega)}{m_2(\omega)}, \forall\omega \in \mathbb{D} \tag{19}$$

with

$$\begin{aligned}m_1(\omega) &= \omega L_{fc}\sin(\omega T_d) - R_{fc}\cos(\omega T_d) \\ &\quad - |G_d(j\omega)|\,\mathrm{Re}\{G_{PR}(j\omega)\}, \end{aligned} \tag{20}$$

$$\begin{aligned}m_2(\omega) &= \omega L_{fc}\cos(\omega T_d) + R_{fc}\sin(\omega T_d) \\ &\quad + |G_d(j\omega)|\,\mathrm{Im}\{G_{PR}(j\omega)\}, \end{aligned} \tag{21}$$

$$\begin{aligned}b(\omega) &= R_{fc}/\,|G_d(j\omega)| + \mathrm{Re}\{G_{PR}(j\omega)\}\cos(\omega T_d) \\ &\quad + \mathrm{Im}\{G_{PR}(j\omega)\}\sin(\omega T_d). \end{aligned} \tag{22}$$

As can be seen, (19) represents a straight line in the complex s-plane for each frequency $\omega_i \in \mathbb{D}$. Using the damped PR controller of Example 2, Fig. 7 exemplarily illustrates filter criteria for distinct frequencies ω_i. Depending on the sign of $m_2(\omega)$, which changes $\leq$ to $\geq$ in (19), the filter's Nyquist plot $H(j\omega)$ has to lie below or above the plotted lines. In this context, the gray areas define regions, where the filter

This article has been accepted for publication in a future issue of this journal, but has not been fully edited. Content may change prior to final publication. Citation information: DOI 10.1109/TIE.2018.2883261, IEEE Transactions on Industrial Electronics

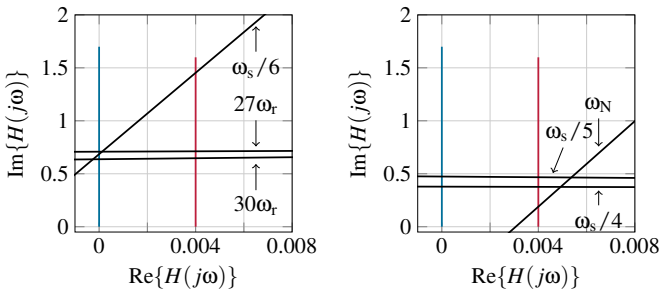

(a) $\omega_i \in [27\,\omega_\mathrm{r}, 30\,\omega_\mathrm{r}, \omega_\mathrm{s}/6]$ (b) $\omega_i \in [\omega_\mathrm{s}/5, \omega_\mathrm{s}/4, \omega_\mathrm{N}]$

Fig. 8: Detailed filter criteria and Nyquist plots of the (blue) D and (red) PD feed-forward filter $H(s)$.

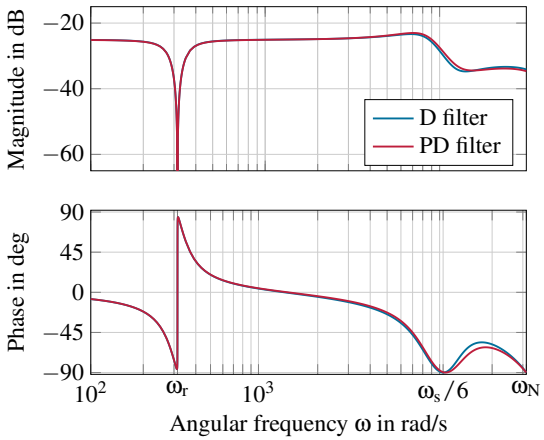

Fig. 9: Bode plots of the VSC input admittance $Y_\mathrm{i}(j\omega)$ using a D and a PD PCC voltage feed-forward filter $H(s)$.

necessarily satisfies (19) for all frequencies in the associated interval. Given the model (6), low frequencies, $\omega \leq 2\,\omega_\mathrm{r}$, are less critical, while (19) imposes more stringent conditions to the filter for high frequencies, $\omega \geq 10/3\,\omega_\mathrm{r}$. As can be observed from Fig. 7c, the filter has to show a phase response $\arg\{H(j\omega)\} \leq 90°$ for frequencies in $[10/3\,\omega_\mathrm{r}, \omega_\mathrm{s}/6]$, but has to tend to $\arg\{H(j\omega)\} \geq 90°$ for high frequencies, see Fig. 7d. Without loss of generality, these characteristics suggest a filter with derivative (D) part, which allows to introduce a phase lead of 90° for high frequencies.

Remark 8: These findings coincide with the observations of [3], but generalize the considerations concerning the PCC feed-forward filter structure from a theoretical point of view.

Remark 9: At this point, it has to be emphasized that a passivity-based filter and controller design must not be limited to high frequency effects, but also has to include effects near the fundamental grid frequency. Recalling that an actively damped VSC consists of a series connection of the system in Fig. 3 and $N(s) = 1 - H(s)G_\mathrm{d}(s)$, it can be verified that $N(s)$ reshapes the original system behavior, shown in Fig. 5. In particular, by adding a feed-forward filter with D part to the system, $N(s)$ introduces an additional phase lag. This may cause non-passive frequency regions of $Y_\mathrm{i}(s)$ close to the resonant frequency. Hence, it is recommended to utilize damped PR controllers, which may impair reference current tracking, but compress the system's phase response close to ω_r, and thus, help to passivate the system. In the context of low switching frequencies, it can also be advantageous to reduce the compensation angle ϕ and in return to increase the resonant cut-off frequency ω_c. Moreover, it should be noted, that phase-locked loops (PLLs) affect the low frequency behavior of the converter input admittance [2], [4], [22], probably resulting in more critical conditions for frequencies $\omega \leq 2\,\omega_\mathrm{r}$.

2) Filter Design: In general, once a PCC feed-forward filter structure has been specified, (19) yields an infinite set of nonlinear inequalities that can be solved for the filter coefficients. However, this procedure may require a high computational effort solving a large number of nonlinear equations. Therefore, in this paper, a more intuitive, successive filter design procedure is proposed, i.e.,

(P1) Select a generic filter of the form

$$H(s) = K_\mathrm{H}\frac{c_m s^m + \ldots + c_1 s + c_0}{r_p s^p + \ldots + r_1 s + 1} \tag{23}$$

where K_H is the proportional gain and $c_0, \ldots c_m$ and $r_1, \ldots r_p$ are the coefficients of the numerator and denominator, respectively.

(P2) For distinct frequencies ω_i, specify reasonable points $H(j\omega_i)$ in the complex s-plane that satisfy (19).

(P3) Determine the proportional gain K_H plus filter coefficients $c_0, \ldots c_m$ and $r_1, \ldots r_p$, such that the filter's Nyquist plot approximates the points of (P2).

(P4) If possible, adapt the filter coefficients, such that (19) is fulfilled for all frequencies $\omega \in \mathbb{D}$. Otherwise go to (P2) and specify new points $H(j\omega_i)$.

Example 3: Suppose Example 2, where a damped PR controller with phase compensation has been designed for a VSC with the parameters of Table I. First, a PD filter of the form $H(s) = K_\mathrm{H}(c_1 s + c_0)$ is considered. Corresponding to Fig. 7c and 7d, Fig. 8 shows exemplary selected filter conditions. Following the proposed procedure, a single point in the complex s-plane is specified, e.g., $H(j\omega_\mathrm{s}/5) = 0.004 + j0.6$. Setting $K_\mathrm{H} = 1$, the coefficients are calculated as $c_0 = 0.004$, $c_1 = 0.6 \cdot 5/\omega_\mathrm{s}$, which yields the filter $H(s) = 0.004 + 4.77 \cdot 10^{-5} s$. As can be observed from the phase response of Fig. 9, the adapted feed-forward filter $H(s)$ renders the input admittance $Y_\mathrm{i}(s)$ strictly passive, i.e., $\arg\{Y_\mathrm{i}(j\omega)\} \in (-90°, 90°), \forall\omega \in \mathbb{D}$.

Example 4: Again suppose the parameters of Example 2. This time, the proposed design procedure shall be applied to a D filter, $H(s) = c_1 s$. In this case, the first term of (19) vanishes, which results in particularly simple criteria. If the influence of the RL filter resistance R_fc and the imaginary part of the PR controller $\mathrm{Im}\{G_\mathrm{PR}(j\omega)\}$ are neglected, (19) can be approximated by $\mathrm{Im}\{H(j\omega)\} \leq K_\mathrm{P}/(\omega L_\mathrm{fc})$ for $\omega \geq \omega_\mathrm{s}/6$. Then, choosing a frequency, e.g., $\omega_i = \omega_\mathrm{s}/6$, yields the coefficient $c_1 = 36\,K_\mathrm{P}/(\omega_\mathrm{s}^2 L_\mathrm{fc}) = 36\,\alpha_\mathrm{c}/\omega_\mathrm{s}^2$. Similar to a PD filter, the resulting D filter $H(s) = 5.4 \cdot 10^{-5} s$ also passivates the input admittance, see Fig. 9.

Remark 10: As can be imagined, there exist system configurations that may result in very stringent passivation design criteria (18), which are hard to satisfy. Regarding sampling effects and the recommendation of [12], similarly harsh con-

This article has been accepted for publication in a future issue of this journal, but has not been fully edited. Content may change prior to final publication. Citation information: DOI 10.1109/TIE.2018.2883261, IEEE Transactions on Industrial Electronics

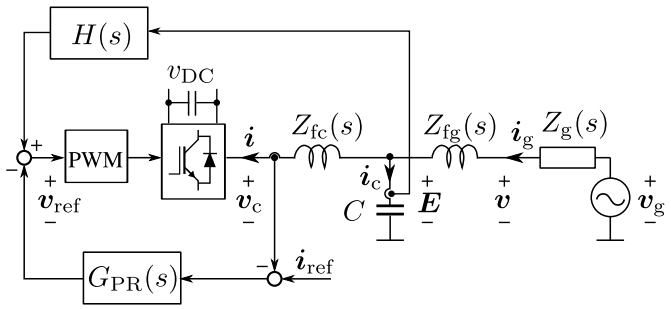

Fig. 10: Single-phase equivalent block diagram of grid-connected VSC with LCL filter and capacitor current feed-forward filter.

ditions may be observed, if safety margins are introduced or the domain $\mathbb{D}$ is extended to frequencies above the Nyquist frequency. To still obtain a non-negative real part of the input admittance up or even above the Nyquist frequency, passive damping must be increased.

C. Extension to LCL output filters

Similar to (17)–(19), the proposed passivation design guidelines can be employed to VSCs that implement LCL output filters and either use converter or grid current feedback [13], [17]. In the latter case, the principle approach of Section IV-A and IV-B keeps the same, where instead of the RL filter admittance $Y_{\mathrm{fc}}(s)$, the transfer function of an LCL filter has to be considered. Since the OFP index of an LCL filter generally depends on the frequency, where it is not possible to factor out the damping resistor, it is also not possible to decompose the filter dynamics into a dynamic part and a static part, as illustrated in Fig. 3. Nevertheless, lower and upper bounds on the OFP index can be deduced, which allow a similar approach as the one presented in the previous sections.

On the other hand, the proposed filter design remains unchanged if converter current feedback is implemented. By contrast, the configuration of Fig. 10 even offers an useful feature, namely that the necessary derivative part of the feed-forward filter $H(s)$ can be avoided [3]. Given Fig. 10 and redefining the voltage $\boldsymbol{E}$ as capacitor voltage, i.e., $\boldsymbol{E}(s) = \frac{1}{Cs}\boldsymbol{i}_{\mathrm{c}}(s) = \frac{1}{Cs}(\boldsymbol{i}(s) - \boldsymbol{i}_{\mathrm{g}}(s))$, where C is the capacitance of the LCL filter and $\boldsymbol{i}_{\mathrm{g}}$ is the current that is injected to the grid, the capacitor current $\boldsymbol{i}_{\mathrm{c}}$ can be used as feed-forward quantity. In this case, the last term of the VSC output voltage $\boldsymbol{v}_{\mathrm{c}}$ in (3) becomes $H(s)\boldsymbol{E}(s) = \frac{H(s)}{Cs}\boldsymbol{i}_{\mathrm{c}}(s)$, and thus, the derivative part of $H(s)$ vanishes. In doing so, the filter capacitance C and the grid side filter impedance $Z_{\mathrm{fg}}(s) = R_{\mathrm{fg}} + sL_{\mathrm{fg}}$ can be added to the grid impedance $Z_{\mathrm{g}}(s)$, i.e. $Z'_{\mathrm{g}}(s) = 1/(Cs) \| (Z_{\mathrm{fg}}(s) + Z_{\mathrm{g}}(s))$ [3]. Since the proposed controller and filter design criteria yield a passive VSC input admittance, which is independent of the grid impedance, (asymptotic) stability is still be guaranteed.

V. Experimental Results

In order to verify the theoretical findings, the proposed feed-forward filter design of Sec. IV-B is applied to a test-system. The experimental-VSC employs an LCL filter and implements converter current control, as depicted in Fig. 10. Table I and II list the system's parameters, where $Z(s) = 0\,\Omega$ and $R_{\mathrm{fg}} = 0\,\Omega$, which results in an effective grid impedance $Z'_{\mathrm{g}}(s) = sL_{\mathrm{fg}}/(s^2 CL_{\mathrm{fg}} + 1)$. Even though $Z'_{\mathrm{g}}(s)$ represents a passive system, the configuration can be considered as a worst-case scenario, since the experimental-VSC is connected to an effective grid impedance that shows an undamped resonance at $\omega_{\mathrm{res}} = 1/\sqrt{CL_{\mathrm{fg}}} = 17.4\,\mathrm{kH}$, lying within the non-passive region of $Y_{\mathrm{i}}(s)$, see the red evolutions in Fig. 5. For the experiments, the PR controller of Example 2 is discretized using Prewarped Tustin, i.e., $G'_{\mathrm{PR}}(z) = (18z^2 - 35.78z + 17.8)/(z^2 - 1.999z + 1)$. In order to avoid a digitally implemented derivation, the capacitor current $\boldsymbol{i}_{\mathrm{c}}$ is used as feed-forward quantity. Then, adopting the results of Example 4, the feed-forward filter is simply given by $H(z) = H(s)/(Cs) = c1/C = 11.5$.

TABLE II: LCL filter parameters

Parameter	Symbol	Value	Units
Converter-side filter inductance	L_{fc}	3	mH
Converter-side filter resistance	R_{fc}	0.2	Ω
Grid-side filter inductance	L_{fg}	0.7	mH
LCL filter capacitance	C	4.7	μF
Filter resonance frequency	ω_{res}	17.4	krad/s
Critical frequency	$\omega_{\mathrm{s}}/6$	10.4	krad/s

Fig. 11 and 12 show the experimental results. In the first scenario, a stepwise change of the current reference from $4\,\mathrm{A}$ to $17\,\mathrm{A}$ is applied to the experimental-VSC. As can be observed, the converter current $\boldsymbol{i}$ shows a overlaid undamped oscillation with a resonance frequency of approximately $3\,\mathrm{kHz}$, if no active passivation is implemented. Contrary, the proposed feed-forward filter $H(z)$ damps the oscillation, resulting in a smoothed converter current. The second scenario, see Fig. 11, demonstrates the stabilizing effect of passivation. If the converter is operated at its nominal current of $18\,\mathrm{A}$ and the feed-forward filter $H(z)$ is disabled, the grid-connected VSC is destabilized by the undamped grid resonance. Hence, it can be seen that stability can be guaranteed by implementing a passive input admittance $Y_{\mathrm{i}}(s)$, which verifies the theoretical findings on the passivation of VSCs with RL as well as LCL output filters.

VI. Conclusion

In this paper, the passivation of current-controlled grid-connected VSCs has been discussed from a system-theoretic point of view. Introducing the concept of passivity indices, it was shown how the converter input admittance can be interpreted as interconnected subsystems. This allows to derive generic and necessary passivation design criteria, which were carried out exemplarily for passive as well as active damping of an VSC with RL output filter. It was discussed, how the results can be adapted to converters that implement LCL filters. Further, it can be stated that, if the input admittance is to be rendered passive, the feed-forward filter design must not be limited to high frequency components, but also has to consider frequencies less than the critical frequency $\omega_{\mathrm{s}}/6$. Finally, experimental results validated the theoretical findings,

This article has been accepted for publication in a future issue of this journal, but has not been fully edited. Content may change prior to final publication. Citation information: DOI 10.1109/TIE.2018.2883261, IEEE Transactions on Industrial Electronics

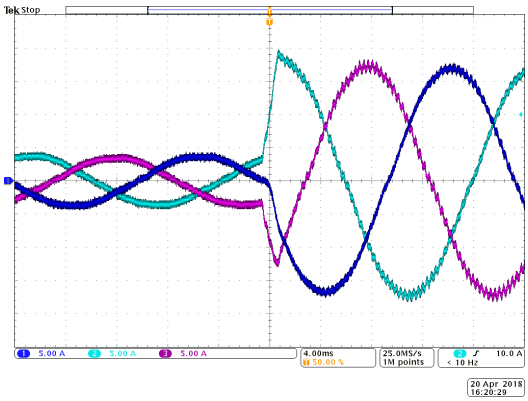

(a)

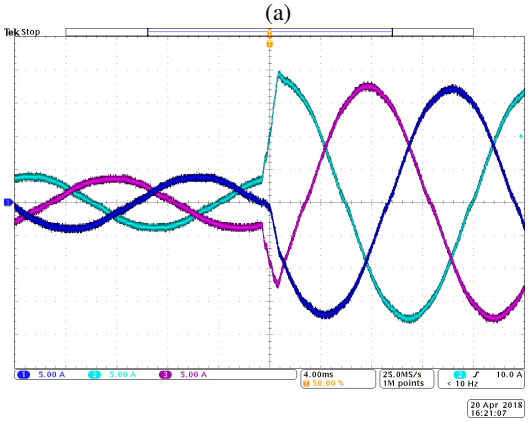

(b)

Fig. 11: Measured current $\boldsymbol{i}$ as a result of a stepwise change of the current reference at $t = 20\,\mathrm{ms}$ (a) without and (b) with feed-forward filter $H(z)$.

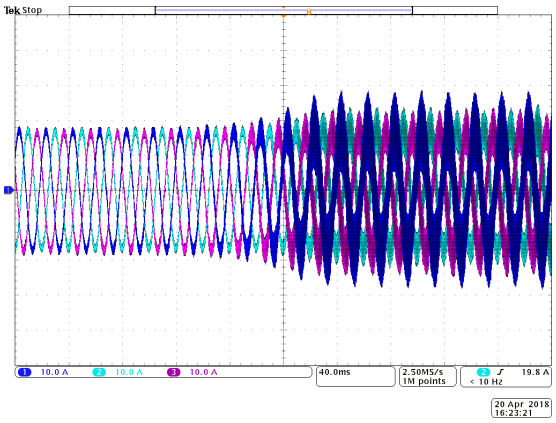

Fig. 12: VSC current response at nominal converter current, if the feed-forward filter $H(z)$ is enabled at the beginning and disabled at $t = 160\,\mathrm{ms}$.

showing that the proposed passivation process stabilizes a current-controlled VSC, which is connected to an undamped grid resonance.

REFERENCES

[1] J. H. Enslin and P. J. Heskes, "Harmonic interaction between a large number of distributed power inverters and the distribution network," *IEEE Trans. Power Electron.*, vol. 19, no. 6, pp. 1586–1593, Nov. 2004.

[2] X. Wang and F. Blaabjerg, "Harmonic stability in power electronic based power systems: concept, modeling, and analysis," *IEEE Trans. Smart Grid, early access*, 2018.

[3] L. Harnefors, A. G. Yepes, A. Vidal, and J. Doval-Gandoy, "Passivity-based controller design of grid-connected VSCs for prevention of electrical resonance instability," *IEEE Trans. Ind. Electron.*, vol. 62, no. 2, pp. 702–710, Feb. 2015.

[4] L. Harnefors, X. Wang, A. G. Yepes, and F. Blaabjerg, "Passivity-based stability assessment of grid-connected VSCs - an overview," *IEEE J. of Emerg. Sel. Topics Power Electron.*, vol. 4, no. 1, pp. 116–125, Mar. 2016.

[5] J. Sun, "Impedance-based stability criterion for grid-connected inverters," *IEEE Trans. Power Electron.*, vol. 26, no. 11, pp. 3075–3078, Nov. 2011.

[6] M. Liserre, R. Teodorescu, and F. Blaabjerg, "Stability of photovoltaic and wind turbine grid-connected inverters for a large set of grid impedance values," *IEEE Trans. Power Electron.*, vol. 21, no. 1, pp. 263–272, Jan. 2006.

[7] S. Vesti, T. Suntio, J. Oliver, R. Prieto, and J. Cobos, "Impedance-based stability and transient-performance assessment applying maximum peak criteria," *IEEE Trans. Power Electron.*, vol. 28, no. 5, pp. 2099–2104, May 2013.

[8] X. Wang, F. Blaabjerg, and W. Wu, "Modeling and analysis of harmonic stability in an ac power-electronics-based power system," *IEEE Trans. Power Electron.*, vol. 29, no. 12, pp. 6421–6432, Feb. 2014.

[9] J. Bao and P. L. Lee, *Process control: the passive systems approach*. Springer-Verlag, 2007.

[10] H. K. Khalil, *Nonlinear Systems: Pearson New International Edition. Always learning*. Pearson Education, Limited, 2013.

[11] L. Harnefors, L. Zhang, and M. Bongiorno, "Frequency-domain passivity-based current controller design," *IET Power Electron.*, vol. 1, no. 4, pp. 455–465, Dec. 2008.

[12] L. Harnefors, R. Finger, X. Wang, H. Bai, and F. Blaabjerg, "VSC input-admittance modeling and analysis above the nyquist frequency for passivity-based stability assessment," *IEEE Trans. Ind. Electron.*, vol. 64, no. 8, pp. 6362–6370, Aug. 2017.

[13] X. Wang, F. Blaabjerg, and P. C. Loh, "Passivity-based stability analysis and damping injection for multiparalleled VSCs with LCL filters," *IEEE Trans. Power Electron.*, vol. 32, no. 11, pp. 8922–8935, Nov. 2017.

[14] M. Aeberhard, M. Meyer, and C. Courtois, "The new standard EN 50388-2 part 2 - stability and harmonics," *Elektrische Bahnen*, vol. 12, no. 1, pp. 28–35, 2014.

[15] X. Zhang, J. W. Spencer, and J. M. Guerrero, "Small-signal modeling of digitally controlled grid-connected inverters with LCL filters," *IEEE Trans. Power Electron.*, vol. 60, no. 9, pp. 3752–3765, Sept. 2013.

[16] D. Holmes, T. Lipo, B. McGrath, and W. Kong, "Optimized design of stationary frame three phase ac current regulators," *IEEE Trans. Power Electron.*, vol. 24, no. 11, pp. 2417–2426, Nov. 2009.

[17] X. Wang, Y. W. Li, F. Blaabjerg, and P. C. Loh, "Virtual-impedance-based control for voltage-source and current-source converters," *IEEE Trans. Power Electron.*, vol. 30, no. 12, pp. 7019–7037, Dec. 2015.

[18] G. F. Franklin, J. D. Powell, and M. L. Workman, *Digital control of dynamic systems*, vol. 3. Addison-wesley Menlo Park, CA, 1998.

[19] L. Harnefors, A. G. Yepes, A. Vidal, and J. Doval-Gandoy, "Multifrequency current control with distortion-free saturation," *IEEE J. of Emerg. Sel. Topics Power Electron.*, vol. 4, no. 1, pp. 37–43, Mar. 2016.

[20] A. G. Yepes, F. D. Freijedo, Ó. Lopez, and J. Doval-Gandoy, "Analysis and design of resonant current controllers for voltage-source converters by means of nyquist diagrams and sensitivity function," *IEEE Trans. Ind. Electron.*, vol. 58, no. 11, pp. 5231–5250, Nov. 2011.

[21] D. N. Zmood and D. G. Holmes, "Stationary frame current regulation of pwm inverters with zero steady-state error," *IEEE Trans. Power Electron.*, vol. 18, no. 3, pp. 814–822, May 2003.

[22] F. Hans, W. Schumacher, and L. Harnefors, "Small-signal modeling of three-phase synchronous reference frame phase-locked loops," *IEEE Trans. Power Electron.*, vol. 33, no. 7, pp. 5556–5560, Jul. 2018.

Florian Hans (S'18) received the Bachelor degree at the university of applied science Kaiserslautern, Germany in 2013 and his Master's degree in electrical engineering from the Technical University Munich, Germany in 2015. He is currently working as research assistant toward his doctoral degree at the Institute of Control Engineering at Technische Universität Braunschweig, Germany.

His research interests include the passivity-based control and analysis of power converters and the stability assessment of power grids employing a large number of distributed renewable energy sources.

Walter Schumacher (M'93) received the Dipl. Ing. degree and the Dr. Ing. degree in electrical engineering from the Technische Universität Braunschweig, Braunschweig Germany in 1979 and 1985 respectively. From 1984 to 1993 he was with the Institute of Applied Microelectronics in Braunschweig, Germany. Since 1993, he is a Full Professor and the Head of the Department of Control Engineering at the Technische Universität Braunschweig.

His research Interests are control of AC drives, mechatronics and power electronics in grids.

Shih-Feng Chou (S'09-M'17) was born in Taipei, Taiwan, in 1987. He received the B.S. and M.S. degrees in electrical engineering from National Tsing Hua University, Hsinchu, Taiwan, in 2009 and 2011, respectively. He had performed R&D in power electronics for renewable energy systems with Delta Electronics, Inc., Taoyuan, Taiwan, from 2012 to 2017. Since 2017, he was a research assistant in the department of energy technology in Aalborg University, Aalborg, Denmark, where he is currently working toward the Ph.D. degree.

His research focuses on modeling of large-scale power electronics based power system.

Xiongfei Wang (S'10-M'13-SM'17) received the B.S. degree from Yanshan University, Qinhuangdao, China, in 2006, the M.S. degree from Harbin Institute of Technology, Harbin, China, in 2008, both in electrical engineering, and the Ph.D. degree in energy technology from Aalborg University, Aalborg, Denmark, in 2013. Since 2009, he has been with the Department of Energy Technology, Aalborg University, where he is currently a Professor and Research Program Leader for Electronic Grid Infrastructure. His research interests include modeling and control of grid-connected converters, harmonics analysis and control, passive and active filters, stability of power electronic based power systems.

Dr. Wang serves as an Associate Editor for the IEEE TRANSACTIONS ON POWER ELECTRONICS, the IEEE TRANSACTIONS ON INDUSTRY APPLICATIONS, and the IEEE JOURNAL OF EMERGING AND SELECTED TOPICS IN POWER ELECTRONICS. In 2016, he was selected into Aalborg University Strategic Talent Management Program for the next-generation research leaders. He received five IEEE prize paper awards, the outstanding reviewer award of IEEE TRANSACTIONS ON POWER ELECTRONICS in 2017, and the IEEE PELS Richard M. Bass Outstanding Young Power Electronics Engineer Award in 2018.